A frameshifting stimulatory stem loop destabilizes the hybrid state and impedes ribosomal translocation

Hee-Kyung Kim[a], Fei Liu[a], Jingyi Fei[b,1], Carlos Bustamante[a,c,d], Ruben L. Gonzalez, Jr.[b], and Ignacio Tinoco, Jr.[a,2]

[a]Department of Chemistry, [c]Department of Physics and Department of Molecular and Cellular Biology, and [d]Howard Hughes Medical Institute, University of California, Berkeley, CA 94720; and [b]Department of Chemistry, Columbia University, New York, NY 10027

Contributed by Ignacio Tinoco, Jr., February 25, 2014 (sent for review January 26, 2014)

Ribosomal frameshifting occurs when a ribosome slips a few nucleotides on an mRNA and generates a new sequence of amino acids. Programmed −1 ribosomal frameshifting (−1PRF) is used in various systems to express two or more proteins from a single mRNA at precisely regulated levels. We used single-molecule fluorescence resonance energy transfer (smFRET) to study the dynamics of −1PRF in the *Escherichia coli dnaX* gene. The frameshifting mRNA (FSmRNA) contained the frameshifting signals: a Shine–Dalgarno sequence, a slippery sequence, and a downstream stem loop. The dynamics of ribosomal complexes translating through the slippery sequence were characterized using smFRET between the Cy3-labeled L1 stalk of the large ribosomal subunit and a Cy5-labeled $tRNA^{Lys}$ in the ribosomal peptidyl-tRNA–binding (P) site. We observed significantly slower elongation factor G (EF-G)–catalyzed translocation through the slippery sequence of FSmRNA in comparison with an mRNA lacking the stem loop, ΔSL. Furthermore, the P-site tRNA/L1 stalk of FSmRNA-programmed pretranslocation (PRE) ribosomal complexes exhibited multiple fluctuations between the classical/open and hybrid/closed states, respectively, in the presence of EF-G before translocation, in contrast with ΔSL-programmed PRE complexes, which sampled the hybrid/closed state approximately once before undergoing translocation. Quantitative analysis showed that the stimulatory stem loop destabilizes the hybrid state and elevates the energy barriers corresponding to subsequent substeps of translocation. The shift of the FSmRNA-programmed PRE complex equilibrium toward the classical/open state and toward states that favor EF-G dissociation apparently allows the PRE complex to explore alternative translocation pathways such as −1PRF.

programmed ribosomal frameshifting | ribosomal dynamics | single-molecule FRET | mRNA secondary structure

The ribosome is the molecular machine that synthesizes proteins by translating messenger RNAs (mRNAs); each sequence of 3 nt, 1 codon, characterizes 1 aa (1–3). Failure to maintain frame during translation occurs with a low error of 10^{-5} (4); however, frameshifting with high efficiency ($>10^{-2}$) is often programmed into many mRNAs to express two or more proteins from a single mRNA (5, 6). Many RNA viruses, including HIV-1, use programmed frameshifting to produce their vital proteins at a precise ratio (7, 8). The common −1 programmed ribosomal frameshifting (−1PRF) signals are a heptanucleotide slippery sequence (X XXY YYZ, underlining denotes the zero-frame) and a downstream stimulatory secondary structure such as a stem loop or a pseudoknot. Frameshifting that takes place on the slippery sequence results in minimal base pair mismatches. Prokaryotic systems have an additional stimulatory signal, an upstream, internal Shine–Dalgarno (SD) sequence (9). The *dnaX* gene of *Escherichia coli* has the three −1PRF signals; an SD sequence, an A AAA AAG slippery sequence, and a downstream stem loop (9–12). Highly efficient (50–80%) −1PRF during translation of the mRNA results in production of the γ DNA-polymerase subunit in the −1 frame and the τ DNA-polymerase subunit in the 0 frame (10).

The −1PRF signals are spaced so that the slippery sequence is positioned within the ribosomal peptidyl-tRNA–binding (P) site and aminoacyl-tRNA–binding (A) site, whereas the downstream secondary structure is positioned at the ribosomal mRNA entry channel (Fig. 1) (5–8, 13). The upstream SD sequence base pairs with 16S ribosomal RNA (rRNA) near the ribosomal tRNA exit (E) site (Fig. 1) (9). Both the SD sequence and the downstream secondary structure can cause pausing during translation (14–19). However, frameshifting efficiency is not strictly related to the pausing extent (15, 17), and it is not proportional to the thermodynamic or mechanical stabilities of the secondary structures (7, 20). Nonetheless, it does correlate with the thermodynamic stability of the first 3–4 bp of the downstream secondary structure (21), and with the conformational plasticity of this structure (7, 20). However, a mechanism by which the stimulatory secondary structure promotes efficient frameshifitng has not emerged yet.

A translational elongation cycle starts with selecting a correct aminoacyl-tRNA in the A site via conformational changes of the posttranslocation (POST) ribosomal complex that are triggered upon binding an EF-Tu(GTP)·aminoacyl-tRNA ternary complex (TC) (1). Once peptidyl transfer takes place, the resulting pretranslocation (PRE) ribosomal complex undergoes large-scale conformational changes that facilitate translocation of the tRNAs from the P and A sites into the E and P sites, simultaneously advancing the ribosome along the mRNA by 3 nt (22). In the first step of translocation, the acceptor stems of the tRNAs are repositioned within the large ribosomal (50S, in prokaryotes) subunit to move the tRNAs from their classical (P/P, A/A) state to their hybrid (P/E, A/P) states, where X and Y in the X/Y notation refer to the position of the anticodon stem loop (ASL) of the tRNA in the small ribosomal (30S, in prokaryotes) subunit and the position of the acceptor stem of the tRNA in the 50S subunit, respectively.

Significance

A ribosomal frameshift occurs when the ribosome slips by one or more nucleotides on the messenger RNA (mRNA) during translation. Programmed ribosomal frameshifting produces more than one protein from a single mRNA and is tightly regulated by mRNA sequence and structure. Using single-molecule fluorescence resonance energy transfer, we studied the effects of a frameshifting stimulatory mRNA structure on the ribosomal conformational dynamics and translocation rate. Our results show that the structure shifts the conformational equilibrium of ribosomal complexes away from conformations that favor the translocation process, resulting in slowed translocation. We propose that the downstream structure traps ribosomal complexes in the fluctuating conformational states of the translocation process and thus allows more opportunities for frameshifting.

Author contributions: H.-K.K., C.B., R.L.G., and I.T. designed research; H.-K.K. performed research; H.-K.K., F.L., J.F., and R.L.G. contributed new reagents/analytic tools; H.-K.K. and I.T. analyzed data; and H.-K.K., C.B., R.L.G., and I.T. wrote the paper.

The authors declare no conflict of interest.

[1]Present address: Center for the Physics of Living Cells, Department of Physics, University of Illinois, Urbana, IL 61801.

[2]To whom correspondence should be addressed. E-mail: intinoco@lbl.gov.

This article contains supporting information online at www.pnas.org/lookup/suppl/doi:10.1073/pnas.1403457111/-/DCSupplemental.

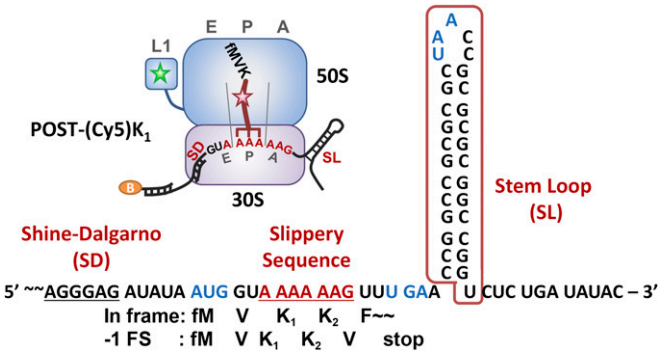

Fig. 1. A programmed −1 FSmRNA construct and a schematic drawing of a ribosomal complex translating the slippery sequence. FSmRNA contains three −1PRF signals from the *dnaX* gene in *E. coli*; an SD sequence, a slippery sequence, and a downstream stem loop. ΔSL mRNA has the same sequence as FSmRNA except with the stem loop (red box) deleted. Start and stop codons are highlighted in blue. Corresponding polypeptide sequences are shown below the mRNA. A schematic drawing of the POST-(Cy5)K_1 complex shows the 50S and 30S subunits in blue and purple rectangles, respectively. The L1 stalk in the small blue rectangle is labeled with Cy3. The ribosomal complex contains fMVK-(Cy5)tRNA^{Lys} in the P site, where the slippery sequence is being displayed. The upstream SD sequence forms base pairs with 16S rRNA and the downstream stem loop presents at the mRNA entry channel in the 30S subunit. The orange oval denotes the biotin on a DNA primer annealed to the 5′ end of the mRNA for immobilization.

Hybrid state (H) formation is accompanied by rotation of the 30S subunit relative to the 50S subunit (23, 24) and a closure of the L1 stalk of the 50S subunit such that it forms a direct contact with the P/E hybrid tRNA (23–25), a global conformation of the PRE complex that we refer to as "global state 2" (25). Global state 1, in contrast, contains classical state (C) tRNAs, nonrotated subunits, and an open L1 stalk (25). Single-molecule fluorescence resonance energy transfer (smFRET) studies of this step of translocation have shown that the H state forms spontaneously upon peptidyl transfer and that, in the absence of an elongation factor-G (EF-G), the H state exists in a dynamic equilibrium with the C state (25–27). Translocation is completed by movement of the ASLs of the tRNAs and the mRNA in the 30S subunit. This step, which comprises the rate-limiting step for the overall process of translocation, requires unlocking of the PRE complex, a conformational change that is thought to involve swiveling of the head domain of the 30S subunit (28, 29) and that is catalyzed by EF-G (30). smFRET and structural studies suggest that the L1 stalk–P/E hybrid tRNA interaction that is established during the first step of translocation is preserved throughout the second step of translocation and is essential for guiding the translocation of the P/E hybrid tRNA into the E site (25, 31, 32).

Here, we report an smFRET study of the dynamics of ribosomal complexes programmed with the −1PRF mRNA of the *E. coli dnaX* gene. We used a FRET pair composed of a Cy3-labeled L1 stalk [L1(Cy3)-stalk] and a Cy5-labeled P-site tRNA^{Lys} [(Cy5)tRNA^{Lys}] on the first lysine codon in the slippery sequence. As previously demonstrated (25), this FRET pair enabled us to monitor transitions of ribosomal complexes between C and H states and the subsequent release of the translocated (Cy5)tRNA^{Lys} from the E site, along one round of the translational elongation cycle. Two mRNA constructs, one containing the downstream stem loop and one lacking it, were compared to study the effect of the secondary structure on the dynamics and translocation of the ribosomal complexes. Our results show that the downstream stem loop changes the dynamics of the PRE ribosomal complexes and disturbs the translocation process. We propose that frameshifting is one of the favorable paths that the ribosome can adopt during the futile EF-G–driven translocation attempts from the H state.

Results

A Downstream Secondary Structure Is Crucial for Efficient Frameshifting. A frameshifting mRNA (FSmRNA) was designed following the −1PRF signals in the *dnaX* gene: an SD sequence, an A AAA AAG slippery sequence coding two tandem lysines (K_1K_2), and a downstream stable stem loop (Fig. 1) (9–12). The SD sequence is positioned 5 nt upstream from the AUG start codon, so that it can play a role as an initiation signal (33) as well as a frameshift-promoting signal. The stem loop was modified to form 12 bp and to have an in-frame stop codon in the loop. A mutant mRNA, ΔSL has the same sequence as the FSmRNA except that the downstream stem loop is deleted. The first 4 aa encoded in both mRNAs are MVK_1K_2. LC–electrospray ionization mass spectrometry analysis on the translated polypeptide products from bulk in vitro translation showed ∼70% frameshifted product in FSmRNA (Fig. S1). This is consistent with in vitro biochemical studies of frameshifting in the *dnaX* gene that show approximately ∼80% frameshifting efficiency (10). ΔSL produced only 4% frameshifted products measured by mass spectrometry, confirming that the stem loop is critical for efficient −1 frameshifting.

FSmRNA-Programmed PRE Complexes Undergo the Same Conformational Changes as ΔSL-Programmed PRE Complexes. POST complexes with fMet-Val-tRNA^{Val} in the P site (POST-V) were enzymatically formed with FSmRNA and ΔSL and immobilized to the surface of flow cells for smFRET measurements (*SI Materials and Methods*). The immobilized POST-V complexes were subjected to one round of translation elongation by successive injections of 100 nM EF-Tu(GTP)·Lys-(Cy5)tRNA^{Lys} TC [TC(Cy5-K)] and 2 μM EF-G(GTP) with washing steps in-between, forming another POST complex with fMet-Val-Lys-(Cy5)tRNA^{Lys} in the P site [POST-(Cy5)K_1] (Fig. 1). The vacant A site in POST-(Cy5)K_1 contained the second lysine codon in the slippery sequence. Most FRET efficiency (E_{FRET}; the acceptor fluorescence intensity divided by the sum of acceptor and donor fluorescence intensity) versus time traces showed a stable, low E_{FRET} state centered at ∼0.2, indicative of stable POST-(Cy5)K_1 complexes (25). One-dimensional E_{FRET} histograms showed that 50–60% of POST-V complexes programmed with either mRNA had formed POST-(Cy5)K_1 (Fig. S2). TC(Cy5-K) did not incorporate into initiation complexes, which displayed a valine codon in the A site, confirming the codon-specific binding of TC(Cy5-K) in the slippery sequence (Fig. S2).

For real-time observations of the peptidyl transfer and translocation processes, 250 nM nonfluorophore labeled TC(K) with 0–1 μM EF-G(GTP) were codelivered to the immobilized POST-(Cy5)K_1 at 10 s after starting imaging (Fig. 2). For both mRNAs, 40–60% of the traces displaying a stable, low E_{FRET} state showed transitions to an E_{FRET} state centered at ∼0.8 upon delivery of the TC(K) and EF-G(GTP) (Fig. 2*B* and Fig. S2). In the absence of EF-G(GTP), the transitions to the ∼0.8 E_{FRET} state were followed by continuous fluctuations between the ∼0.2 and ∼0.8 E_{FRET} states (Fig. S3). These observations indicate that peptidyl transfer took place, forming a PRE complex containing a deacylated (Cy5)tRNA^{Lys} in the P site and a peptidyl-tRNA^{Lys} in the A site [PRE-(Cy5)K_1K_2]; the PRE complexes programmed with either mRNA were undergoing conformational transitions between the H (high, ∼0.8 E_{FRET}) and the C (low, ∼0.2 E_{FRET}) states as demonstrated previously (Fig. 2*A*) (25).

The Downstream Stem Loop Does Not Affect the Peptidyl Transfer Process, but Does Affect the Stability of the H State. The duration between TC(K) delivery and the first transition to the high, ∼0.8 E_{FRET} state (t_{pt} in Fig. 2*B*) corresponds to the time for a series of events, including TC(K) binding, peptidyl transfer, and the first conformational transition to the H state. Consistent with this, the t_{pt} histograms showed Poisson distributions with two rate-limiting steps for both FSmRNA- and ΔSL-programmed

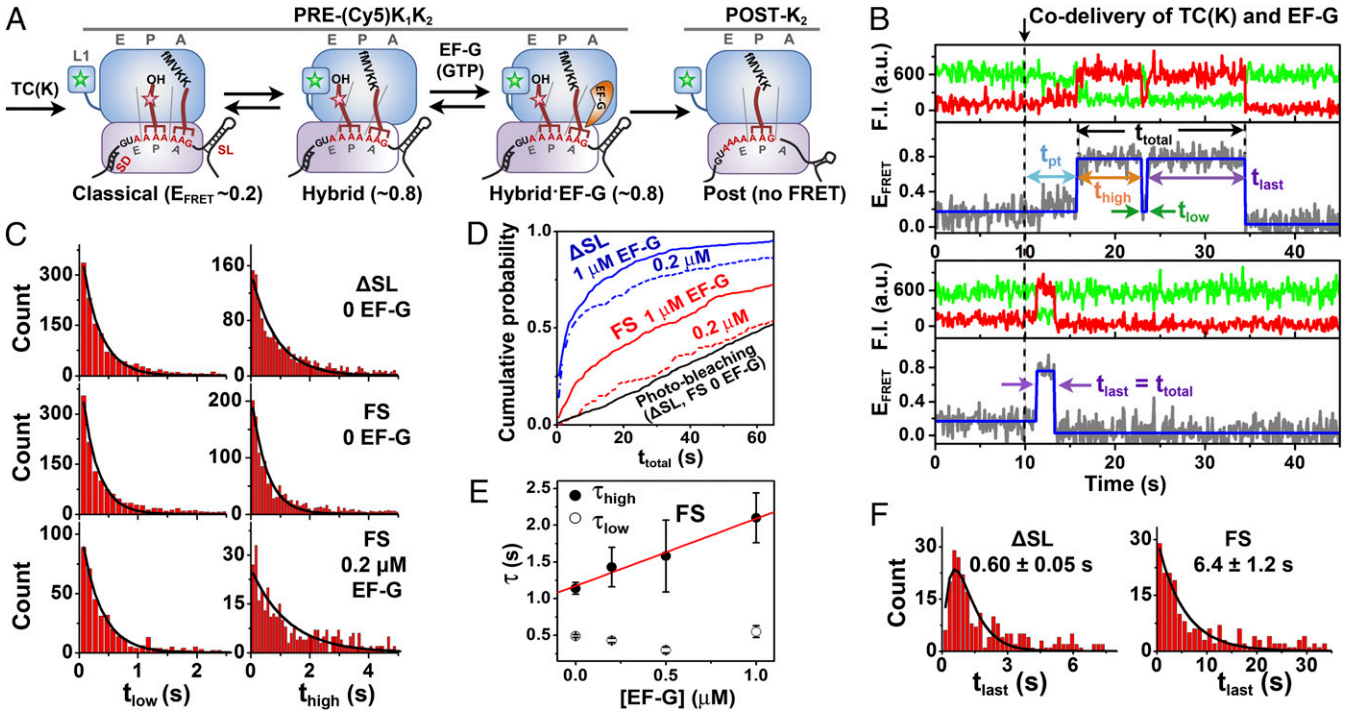

Fig. 2. smFRET measurements. (*A*) Schematic drawings of the ribosomal complexes along one cycle of translational elongation. Peptidyl transfer upon binding of a cognate TC, TC(K), forms the PRE-(Cy5)K_1K_2 complex, which is in dynamic equilibrium between the C (E_{FRET} ~0.2) and H (E_{FRET} ~0.8) states. The G state (Hybrid·EF-G) displays the same E_{FRET} as the H state. EF-G–catalyzed translocation and subsequent release of (Cy5)$tRNA^{Lys}$ results in the formation of the POST-K_2 complex. (*B*) Representative time traces of fluorescence intensity (F.I.) (Cy3 in green and Cy5 in red) of POST-(Cy5)K_1 with either FSmRNA (*Upper*) or ΔSL (*Lower*) upon delivery of 250 nM TC(K) and 0.2 μM EF-G(GTP) at 10 s. Corresponding E_{FRET} in gray was fit to the hidden Markov model shown in blue. t_{pt} is the duration from TC(K) delivery to the first transition to the high E_{FRET} upon peptidyl transfer. (*C*) Dwell time histograms of low (t_{low}, *Left*) and high (t_{high}, *Right*) E_{FRET} states of $PRE_{\Delta SL}$ (*Top*) and PRE_{FS} (FS, *Middle*) in the absence of EF-G. (*Bottom*) Dwell time histograms of PRE_{FS} in the presence of 0.2 μM EF-G. The histograms were fitted to single exponential decay curves. The time resolution was 50 ms per frame. (*D*) Cumulative probabilities of t_{total} at 0, 0.2, and 1 μM EF-G for $PRE_{\Delta SL}$ (blue) and PRE_{FS} (red). (*E*) Mean dwell times of the high (τ_{high}) and low (τ_{low}) E_{FRET} state of the PRE_{FS} at various EF-G concentrations with 100 ms per frame time resolution. The error bars are standard deviations of the means calculated by a block bootstrapping method (*SI Materials and Methods*). (*F*) Dwell time histograms of the last high E_{FRET} state (t_{last}) transiting to no FRET in the presence of 1 μM EF-G. t_{last} of $PRE_{\Delta SL}$ were described with Poisson distributions with two rate-limiting steps, whereas t_{last} of PRE_{FS} followed a single exponential decay.

ribosomal complexes (Fig. S4). No substantial differences of the rates were observed between the two complexes (Table 1), suggesting that the downstream stem loop does not induce noticeable changes on the peptidyl transfer process.

Table 1. Summary of the mean dwell times and number of fluctuations for the $PRE_{FS/\Delta SL}$ complexes

Time resolution	mRNA	[EF-G], μM	n (fluctuating)*	τ_{pt}, s	N†	τ_{low}, s	τ_{high}, s	τ_{last}, s	τ_{total}, s‡
50 ms	ΔSL	0	233 (94%)	2.5 ± 0.2		0.30 ± 0.04	0.93 ± 0.21		
	FS	0	200 (93%)	2.1 ± 0.2		0.28 ± 0.02	0.52 ± 0.12		
		0.2	159 (75%)	2.0 ± 0.1		0.33 ± 0.04	1.15 ± 0.39		
100 ms	ΔSL	0	486 (92%)		(11)	0.48 ± 0.02	1.10 ± 0.07		
		0.1	274 (37%)		(1.6)			0.88 ± 0.10	1.28 ± 0.13
		0.2	251 (29%)		(1.5)			0.92 ± 0.07	1.09 ± 0.09
		0.5	236 (23%)		(1.2)			0.48 ± 0.04	0.48 ± 0.04
		1	298 (22%)		(1.2)			0.60 ± 0.05	0.65 ± 0.07
	FS	0	319 (94%)		(10)	0.49 ± 0.02	1.14 ± 0.08		
		0.2	123 (76%)		3.4 (4.8)	0.43 ± 0.03	1.43 ± 0.27		
		0.5	87 (63%)		1.9 (2.9)	0.30 ± 0.04	1.58 ± 0.49		
		1	316 (49%)		1.0 (2.3)	0.55 ± 0.08	2.10 ± 0.34	6.4 ± 1.2	18 ± 4

Mean dwell times were obtained from single exponential decay fittings except that τ_{last} and τ_{total} for ΔSL and τ_{pt} for the both mRNAs were obtained from fitting to Poisson distributions with two identical rate-limiting steps (Fig. 2*C* and Figs. S5 and S7). Mean dwell times in the absence of EF-G are averages of three replicates and errors are their standard deviations. Mean dwell times and the errors (standard deviations) in the presence of EF-G are obtained by a block bootstrapping method (*SI Materials and Methods*).

*The total numbers of traces collected from 1 to 4 replicates are n; in parentheses (fluctuating) are the percentages of traces visiting the high E_{FRET} state more than once before losing Cy5 signal.

†N is the mean number of transitions to the high E_{FRET} state per trace obtained from fitting to single exponential decay curves; in parentheses are the arithmetic averaged N for the traces in 95% of the population (Figs. S5 and S7).

‡τ_{total} values were corrected for photobleaching rate by $1/\tau_{total} = 1/\tau_{total,\ obs} - 1/\tau_{photobleaching}$.

The dwell times of the C (low, ~0.2 E_{FRET}) and the H (high, ~0.8 E_{FRET}) states of the PRE-(Cy5)K_1K_2 complexes in the absence of EF-G were well described with single exponential decay curves (Fig. 2*C*). In comparison with ΔSL-programmed PRE ($PRE_{\Delta SL}$) complexes, FSmRNA-programmed PRE (PRE_{FS}) complexes displayed considerably shorter dwells on the H state ($\tau_{high,\ \Delta SL} = 0.93 \pm 0.21$ s versus $\tau_{high,\ FS} = 0.52 \pm 0.12$ s), whereas no substantial difference was observed for the C state dwells ($\tau_{low,\ \Delta SL} = 0.30 \pm 0.04$ s versus $\tau_{low,\ FS} = 0.28 \pm 0.02$ s). These observations indicate that the downstream stem loop effectively destabilizes the H state. The equilibrium constants, K = [H]/[C], defined by the ratio of the dwell times (τ_{high}/τ_{low}) show that PRE_{FS} complexes exhibit an equilibrium that is shifted toward the C state in comparison with $PRE_{\Delta SL}$ complexes ($K_{\Delta SL} = 3.1 \pm 0.2$ versus $K_{FS} = 1.9 \pm 0.1$, errors are propagated errors).

Slow Translocation of PRE_{FS} Complexes Occurs with Characteristic Fluctuations. Translocation of (Cy5)$tRNA^{Lys}$ into the E site and its release thereafter results in the disappearance of the Cy5 signal from the high, ~0.8 E_{FRET} state (POST-K_2 in Fig. 2). To distinguish the release of (Cy5)$tRNA^{Lys}$ upon translocation from photobleaching of Cy5, lower excitation power was used together with a lower time resolution of 100 ms per frame. Translocation in the absence of EF-G is very slow (~10^{-2} to 10^{-4} s^{-1}) (3, 34), and thus the Cy5 signal disappearance upon delivery of TC(K) in the absence of EF-G is mostly due to photobleaching events. Both PRE_{FS} and $PRE_{\Delta SL}$ complexes showed similar long duration from the first high, ~0.8 E_{FRET} state to the disappearance of the Cy5 signal (t_{total}), resulting in ~60-s Cy5 photobleaching half-lives (Fig. 2*D*).

In contrast, ~70% of the traces recorded in the presence of 0.2 μM EF-G(GTP) for $PRE_{\Delta SL}$ complexes rapidly lost the Cy5 signals after a single transition to the high, ~0.8 E_{FRET} state (Fig. 2*B*, *Lower*). The mean duration from the first high, ~0.8 E_{FRET} state to the disappearance of the Cy5 signal ($\tau_{total} = 1.09 \pm 0.09$ s), obtained from fitting to a Poisson distribution with two identical rate-limiting steps (Fig. S5*A*), is ~60-fold shorter than the Cy5 half-life (~60 s) (Fig. 2*D*). The τ_{total} decreased with increasing EF-G(GTP) concentrations up to 0.5 μM and leveled (Table 1). These results indicate that the disappearance of the Cy5 signal in the presence of EF-G(GTP) corresponds to release of (Cy5)$tRNA^{Lys}$ upon translocation. The observation of a single transition to the high, ~0.8 E_{FRET} state before the disappearance of the Cy5 signal, unlike the continuous fluctuations between the high, ~0.8 and low, ~0.2 E_{FRET} states in the absence of EF-G, is consistent with previous reports that binding of EF-G to PRE complexes stabilizes the H state of the PRE complex, from which translocation takes place rapidly (25, 27, 35). The Poisson distributions of t_{total} are consistent with the fact that translocation takes place via multiple steps (22, 36, 37).

PRE_{FS} complexes showed substantially different behavior in comparison with $PRE_{\Delta SL}$ complexes. The mean total time, τ_{total}, at 1 μM EF-G(GTP) was more than 10- to 20-fold longer for the PRE_{FS} compared with that of $PRE_{\Delta SL}$ (Fig. 2*D* and Table 1). Instead of a Poisson distribution as in the $PRE_{\Delta SL}$ complexes, t_{total} was better described by a single exponential decay function (Fig. S6). Below 0.5 μM EF-G(GTP), t_{total} was too long to be accurately measured with the limited Cy5 lifetimes. Furthermore, in contrast to the 70% of the $PRE_{\Delta SL}$ complex traces that showed a single transition to the high, ~0.8 E_{FRET} state before translocation at 0.2 μM EF-G(GTP), 76% of the PRE_{FS} complex traces were still fluctuating between the C and H states at the same EF-G(GTP) concentration (Fig. 2*B*, *Upper*). The percentage of fluctuating PRE_{FS} complex traces decreased as EF-G(GTP) concentration increased, but ~50% of the traces were still fluctuating even at 1 μM EF-G(GTP) (Table 1).

The mean dwell times of the high (τ_{high}) and low (τ_{low}) E_{FRET} states in the PRE_{FS} complexes were compared as a function of EF-G(GTP) concentration. All of the dwell time histograms were well described by single exponential decay curves (Fig. 2*C* and Fig. S7). At a time resolution of 50 ms per frame, a more than twofold lengthened τ_{high} was observed in the presence of 0.2 μM compared with 0 EF-G(GTP) (Fig. 2*C* and Table 1). Experiments with 100 ms per frame time resolution clearly showed that τ_{high} linearly increased with EF-G(GTP) concentration (Fig. 2*E* and Table 1), although dwell time distributions shifted toward longer dwells compared with the results with 50 ms per frame time resolution due to missing short-lived transitions. These results indicate that EF-G binds to the H state. Accordingly, the number of transition to the high, ~0.8 E_{FRET} state per trace (N) decreased as τ_{high} increased (Table 1). Our results suggest that each dwell at the high, ~0.8 E_{FRET} is composed of several cycles of EF-G–binding and dissociation events instead of a single, stable sampling of the H state. In addition, the fact that we see no substantial change in τ_{low} as a function of EF-G concentration implies that effective binding and dissociation of EF-G takes place primarily when the PRE_{FS} complex is in the H state (Fig. 2*E*).

An Additional Rate-Limiting Step Occurs in the Last High, ~0.8 E_{FRET} Dwell. For the majority of $PRE_{\Delta SL}$ complex traces, all of the steps required for translocation took place during the last dwell in the high, ~0.8 E_{FRET} state ($t_{total} = t_{last}$ in Fig. 2*B*, *Lower*). Consistently, t_{last} of ΔSL showed Poisson distributions approaching the distributions of t_{total} at 0.5–1μM EF-G(GTP), at which 80% of the traces showed a single transition to the high, ~0.8 E_{FRET} state (Fig. 2*F* and Table 1). In contrast, t_{last} for PRE_{FS} complexes at 1 μM EF-G(GTP) showed a single exponential distribution ($\tau_{last} = 6.4 \pm 1.2$ s) and was ~10-fold longer compared with $PRE_{\Delta SL}$ complexes (Fig. 2*F*). Moreover, it is almost threefold longer than τ_{high} (2.10 ± 0.34 s). At lower EF-G concentrations, most of the PRE_{FS} traces photobleached before completing translocation, preventing accurate measurements of t_{last}. The facts that τ_{last} for PRE_{FS} complexes is longer than τ_{high} and t_{last} follows a single exponential decay imply the existence of an additional intermediate state (I) that is observed only in the last dwell. Formation of I is irreversible and thus results in forward translocation. Transition from I to the final state, where (Cy5)$tRNA^{Lys}$ has been released, is apparently a rate-limiting step in the translocation of PRE_{FS} complexes, explaining the measured long τ_{last}.

A proposed reaction scheme based on our observations is shown in Fig. 3*A*. The C state is probed by the low, ~0.2 E_{FRET} state. In contrast, the H, EF-G–bound hybrid (G), and I states are indistinguishably probed by the high, ~0.8 E_{FRET} state. Post is a POST complex with an empty E site after releasing (Cy5)$tRNA^{Lys}$, and thus it does not exhibit any FRET. The reaction rates for each step shown in Fig. 3*A* were calculated from the mean dwell times and N measured at different EF-G(GTP) concentrations (Table 2; see details in *SI Equations* and Table S1).

Discussion

The Downstream Secondary Structure Modulates the Free-Energy Landscape of Translocation. Accumulated information on the structures and dynamics of ribosomal complexes suggest that the conformational changes that occur during the translocation process are diffusive between the energy minima along a free-energy landscape (2, 22, 38). Such Brownian conformational fluctuations are rectified by EF-G binding followed by GTP hydrolysis for forward translocation. Here, we demonstrate that downstream, frameshift-stimulating secondary structures can shift the dynamic conformational equilibrium of ribosomal complexes by modulating the free-energy landscape. As shown in the proposed reaction scheme (Fig. 3), our data imply that the slow translocation of PRE_{FS} complexes involves EF-G binding and dissociation events as well as conformational fluctuations between the H and C states.

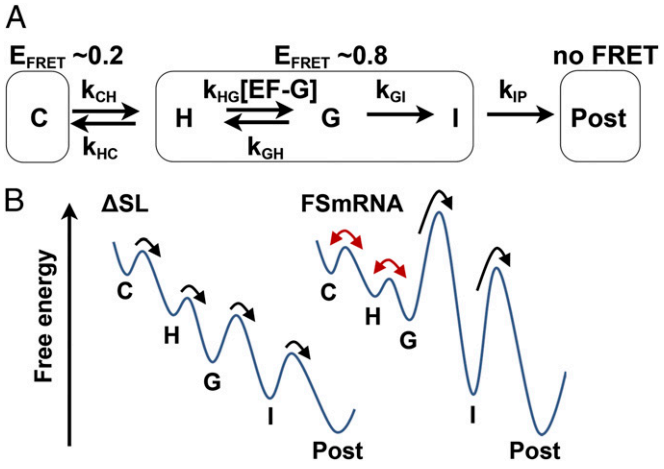

Fig. 3. A proposed reaction scheme and free-energy landscapes of the translocation. (*A*) C, H, and G denote the classical, hybrid, and hybrid·EF-G states that PRE complexes can dynamically visit. I is an intermediate state, from which the reaction becomes irreversible. "Post" denotes the POST complex with an empty E site (POST-K_2, Fig. 2*A*). (*B*) Free-energy landscapes along the translocation for $PRE_{\Delta SL}$ and PRE_{FS} based on the measured reaction rates (Table 2). The energetic barrier between H and G and the energies of the G, I, and Post states are not quantitative. Reversible transitions are highlighted by the red arrows.

The calculated rates of the G-to-I transitions (k_{GI}) and of the I-to-Post transitions (k_{IP}) for the PRE_{FS} complexes ($0.20 \le k_{GI} \le 0.48$, $0.13 < k_{IP} < 0.30\ s^{-1}$) are much slower than the reaction rates of the $PRE_{\Delta SL}$ complexes ($1.9 \pm 0.3\ s^{-1}$) (Table 2 and *SI Equations*), which were obtained from the Poisson fitting of the t_{last} with two rate determining steps (Fig. 2*F*). The results indicate that the frameshifting stimulatory stem loop elevated the energetic barriers for the G-to-I and I-to-Post transitions along the translocation process of PRE_{FS} complexes. With the high barrier toward the I state, the backward steps, EF-G dissociation (k_{GH}) and transition to the C state (k_{HC}) become competitive with the forward step (k_{GI}), in contrast to $PRE_{\Delta SL}$ complexes in which the forward steps are dominant on the downhill energy landscape (Fig. 3*B*). Our model implies that PRE_{FS} complexes require more EF-G–binding events than $PRE_{\Delta SL}$ complexes for a single productive translocation event. The result is similar to the observations of increased futile EF-G binding events with lengthened dwell times in the presence of antibiotics (36). Compared with a previous smFRET study showing three- to fourfold decreased translocation rates by the presence of downstream structures without the upstream SD sequence and slippery sequence (39), our results show more severe effects (>10-fold) of the stem loop on the translocation rate. Further study is needed to learn the relative contribution of each frameshifting element.

During the highly dynamic, multistep translocation process, unlocking of the PRE complex was proposed as a rate-limiting step that likely involves swiveling of the head domain of the 30S subunit and opening of the gate between the P and E sites of the 30S subunit (22, 30). This allows the ASLs of the P- and A-site tRNAs, and the mRNA codons that are base-paired to them, to be translocated into the P and E sites of the 30S subunit (22, 28, 30, 40). Relative to $PRE_{\Delta SL}$ complexes, unwinding of the FSmRNA secondary structure at the ribosomal mRNA entry channel in PRE_{FS} complexes is likely an additional rate-limiting step for translocation (41, 42). Assuming that the I state is a PRE state, the two rate-limiting steps of G-to-I and I-to-Post transitions may involve unlocking of the ribosomal complex and unwinding of the secondary structure. If, on the other hand, the I state is a POST state that precedes the release of $(Cy5)tRNA^{Lys}$ from the E site, the slow k_{IP} means that the downstream stem loop impedes not only translocation, but also E-site tRNA release. This would be consistent with a previous proposal that downstream secondary structures allosterically delay E-site tRNA release (39).

Table 2. Estimated reaction rates of the translocation substeps

mRNA	k_{CH}, s^{-1}*	k_{HC}, s^{-1}†	k_{HG}, $s^{-1}\cdot\mu M^{-1}$	k_{GH}, s^{-1}	k_{GI}, s^{-1}	k_{IP}, s^{-1}
ΔSL	3.3 ± 0.5	1.1 ± 0.3	ND	ND	1.9 ± 0.3‡	1.9 ± 0.3‡
FS	3.6 ± 0.3	1.9 ± 0.5	ND	ND	0.20–0.48§	0.13–0.30¶

ND, k_{HG} and k_{GH} were not determined.
*$k_{CH} = 1/\tau_C$.
†$k_{HC} = 1/\tau_{H0}$ at 0 EF-G.
‡k_{GI} and k_{IP} from Poisson fitting of t_{last} at 1 μM EF-G (Fig. 2*F*).
§$1/[N\cdot\tau_{high} - (N-1)\cdot\tau_{H0}] \le k_{GI} \le 1/[N\cdot\tau_{high} - 2N/(2N-1)\cdot(N-1)\cdot\tau_{H0}]$ (Table S1).
¶$1/\tau_{last} < k_{IP} < 1/(\tau_{last} - \tau_{high})$ at 1 μM EF-G (see *SI Equations*).

Structural Insights into the H State with a Downstream Secondary Structure. Recent cryo-EM and crystal structures of PRE complex analogs lacking an A site-bound peptidyl-tRNA trapped in EF-G–bound, intermediate H states showed that the P-site tRNA is still in contact with the P site of the swiveled head domain of the 30S subunit, while it makes new contacts with the E site of the body domain of the 30S subunit, placing the P-site tRNA somewhere between the P and E sites of the 30S subunit (28, 32, 43, 44). In these structures, repositioning of the P-site tRNA within the 30S subunit pulls the mRNA that is base-paired to the P-site tRNA by 2–3 nt in the direction of translocation. This pulling of the mRNA that accompanies swiveling of the head domain of the 30S subunit will exert mechanical force against the downstream secondary structure (42) and activate the ribosomal helicase activity to unwind it (41). The developed tension would likely interfere with the mRNA–tRNA, mRNA–ribosome, tRNA–ribosome, and ribosome–ribosome interactions that are responsible for stabilizing the H state, resulting in the destabilized H state that we observe. The lack of analogous changes to the stability of the C state indicates that the stem does not affect the C state. This can explain why ribosomal complexes programmed with FSmRNA do not exhibit a change in the rate of peptidyl transfer following delivery of an aminoacyl-tRNA into the A site, events which take place while the tRNAs are in their C states. The tension developed in the H state could also impair the ability of EF-G domain IV to form critical interactions with the A site of the 30S subunit for the efficient translocation (32, 43, 44), thereby resulting in futile EF-G–binding events and inefficient translocation as observed in this study.

One of the crystal structures of the EF-G–bound, intermediate H states has also shown that two universally conserved 16S rRNA bases can intercalate into the mRNA bases in the 30S subunit (43). This interaction has been proposed to play a role in reading frame maintenance during the dynamic conformational changes associated with translocation (43). The observed intercalation interaction might be impaired in a strained mRNA under the tension that is generated upon swiveling of the 30S head domain against frameshift-stimulating secondary structures. In addition, codon–anticodon interactions might be weakened under the tension that is generated while the tRNAs are in the H state, facilitating the deformation of these base-pairing interactions. Under the condition that the frame registry is disrupted, the nature of the slippery sequence is such that the tRNA anticodons can reform base pairs with the slippery sequence in any frame without producing a significant number of base pair mismatches. Thus, not only does −1PRF take place with a minimal energetic penalty of breaking and reforming the codon–anticodon interactions on the slippery sequence, but also relieves the tension on the mRNA by 1 nt. Thus, a −1 frameshift constitutes an alternative path that the ribosome can adopt when it encounters a −1PRF signal. In the

dnaX gene, −1 frameshifting results in Watson–Crick base pairs for both P- and A-site $tRNA^{Lys}$ (A AAA AAG versus AAA AAA G), providing a small energetic gain to the frameshifted conformation, possibly explaining the high frameshifting efficiency of this −1PRF signal.

In summary, our observation of the slow translocation of PRE_{FS} complexes is consistent with biochemical studies showing ribosomal pausing on slippery sequences with downstream secondary structures (15–19). We further determined that pausing is mostly due to the decreased rate of translocation, without changes to the rates of A-site tRNA delivery or peptidyl transfer. Our results show that the downstream stem loop not only elevates the energetic barriers that characterize substeps of the translocation reaction, but that it also destabilizes the H state. It likely also destabilizes the G state as discussed. The energetic barrier to −1 frameshifting becomes lower by the amount of destabilization of the H state with or without EF-G bound. On the modified free-energy landscape, the PRE complex is allowed more time to transit between the C-, H-, and EF-G–bound and EF-G–unbound states before completing translocation. During these dynamic transitions, frameshifting may become an alternative path that the ribosome can adopt.

Materials and Methods

Reconstituted 70S-L1(Cy3) and (Cy5)$tRNA^{Lys}$ were prepared as described in the published protocols (25, 26). mRNAs were prepared by in vitro run off transcriptions on synthetic DNAs using T7 promoter. POST-V complexes were enzymatically formed in the Tris·polymix buffer [50 mM Tris·OAc (pH 7.5), 100 mM KCl, 5 mM NH_4OAc, 0.5 mM $Ca(OAc)_2$, 0.1 mM EDTA, 6 mM 2-mercaptoethanol, 5 mM putrescine and 1mM spermidine] at 10 mM $Mg(OAc)_2$. Biotinylated DNA primer was annealed to the 5′ end of the mRNAs for surface immobilization. For smFRET experiments, diluted POST-V complexes (200–500 pM) were immobilized to a PEG-passivated flowcell via streptavidin–biotin interactions (26). A laboratory-built TIRF microscope equipped with a multichannel imaging system was used for smFRET measurements. Tris·polymix buffer was supplemented with an oxygen-scavenging system (300 μg/mL glucose oxidase, 40 μg/mL catalase, and 1% β-D-glucose; Sigma) and a triplet-state quenching mixture [1 mM 1,3,5,7-cyclooctatetraene (Aldrich), 1 mM *p*-nitrobenzyl alcohol (Fluka), 1.5 mM Trolox (Sigma)] for smFRET experiments (details in *SI Materials and Methods*).

ACKNOWLEDGMENTS. We thank Laura Lancaster and Harry F. Noller (University of California, Santa Cruz) for providing initiation factor proteins and S-100 enzymes, and Shannon Yan for helpful comments. This study is supported by National Institutes of Health (NIH) Grant GM10840 (to I.T.); Burroughs Welcome Fund Career Awards in the Biomedical Sciences CABS 1004856, National Science Foundation CAREER Award MCB 0644262, and NIH Grant R01 GM084288 (to R.L.G.); and NIH Grant 5R01 GM32543 (to C.B.).

1. Schmeing TM, Ramakrishnan V (2009) What recent ribosome structures have revealed about the mechanism of translation. *Nature* 461(7268):1234–1242.
2. Frank J, Gonzalez RL, Jr. (2010) Structure and dynamics of a processive Brownian motor: The translating ribosome. *Annu Rev Biochem* 79:381–412.
3. Moore PB (2012) How should we think about the ribosome? *Annu Rev Biophys* 41: 1–19.
4. Kurland CG (1992) Translational accuracy and the fitness of bacteria. *Annu Rev Genet* 26:29–50.
5. Farabaugh PJ (1996) Programmed translational frameshifting. *Microbiol Rev* 60(1): 103–134.
6. Gesteland RF, Atkins JF (1996) Recoding: Dynamic reprogramming of translation. *Annu Rev Biochem* 65:741–768.
7. Giedroc DP, Cornish PV (2009) Frameshifting RNA pseudoknots: Structure and mechanism. *Virus Res* 139(2):193–208.
8. Brierley I, Dos Ramos FJ (2006) Programmed ribosomal frameshifting in HIV-1 and the SARS-CoV. *Virus Res* 119(1):29–42.
9. Larsen B, Wills NM, Gesteland RF, Atkins JF (1994) rRNA-mRNA base pairing stimulates a programmed -1 ribosomal frameshift. *J Bacteriol* 176(22):6842–6851.
10. Tsuchihashi Z, Kornberg A (1990) Translational frameshifting generates the gamma subunit of DNA polymerase III holoenzyme. *Proc Natl Acad Sci USA* 87(7):2516–2520.
11. Tsuchihashi Z, Brown PO (1992) Sequence requirements for efficient translational frameshifting in the Escherichia coli dnaX gene and the role of an unstable interaction between tRNA(Lys) and an AAG lysine codon. *Genes Dev* 6(3):511–519.
12. Larsen B, Gesteland RF, Atkins JF (1997) Structural probing and mutagenic analysis of the stem-loop required for Escherichia coli dnaX ribosomal frameshifting: Programmed efficiency of 50%. *J Mol Biol* 271(1):47–60.
13. Tinoco I, Jr., Kim HK, Yan S (2013) Frameshifting dynamics. *Biopolymers* 99(12): 1147–1166.
14. Li GW, Oh E, Weissman JS (2012) The anti-Shine-Dalgarno sequence drives translational pausing and codon choice in bacteria. *Nature* 484(7395):538–541.
15. Kontos H, Napthine S, Brierley I (2001) Ribosomal pausing at a frameshifter RNA pseudoknot is sensitive to reading phase but shows little correlation with frameshift efficiency. *Mol Cell Biol* 21(24):8657–8670.
16. Somogyi P, Jenner AJ, Brierley I, Inglis SC (1993) Ribosomal pausing during translation of an RNA pseudoknot. *Mol Cell Biol* 13(11):6931–6940.
17. Tu C, Tzeng TH, Bruenn JA (1992) Ribosomal movement impeded at a pseudoknot required for frameshifting. *Proc Natl Acad Sci USA* 89(18):8636–8640.
18. Lopinski JD, Dinman JD, Bruenn JA (2000) Kinetics of ribosomal pausing during programmed -1 translational frameshifting. *Mol Cell Biol* 20(4):1095–1103.
19. Tholstrup J, Oddershede LB, Sørensen MA (2012) mRNA pseudoknot structures can act as ribosomal roadblocks. *Nucleic Acids Res* 40(1):303–313.
20. Ritchie DB, Foster DA, Woodside MT (2012) Programmed -1 frameshifting efficiency correlates with RNA pseudoknot conformational plasticity, not resistance to mechanical unfolding. *Proc Natl Acad Sci USA* 109(40):16167–16172.
21. Mouzakis KD, Lang AL, Vander Meulen KA, Easterday PD, Butcher SE (2013) HIV-1 frameshift efficiency is primarily determined by the stability of base pairs positioned at the mRNA entrance channel of the ribosome. *Nucleic Acids Res* 41(3):1901–1913.
22. Rodnina MV, Wintermeyer W (2011) The ribosome as a molecular machine: The mechanism of tRNA-mRNA movement in translocation. *Biochem Soc Trans* 39(2): 658–662.
23. Valle M, et al. (2003) Locking and unlocking of ribosomal motions. *Cell* 114(1): 123–134.
24. Agirrezabala X, et al. (2012) Structural characterization of mRNA-tRNA translocation intermediates. *Proc Natl Acad Sci USA* 109(16):6094–6099.
25. Fei J, Kosuri P, MacDougall DD, Gonzalez RL, Jr. (2008) Coupling of ribosomal L1 stalk and tRNA dynamics during translation elongation. *Mol Cell* 30(3):348–359.
26. Blanchard SC, Kim HD, Gonzalez RL, Jr., Puglisi JD, Chu S (2004) tRNA dynamics on the ribosome during translation. *Proc Natl Acad Sci USA* 101(35):12893–12898.
27. Cornish PV, Ermolenko DN, Noller HF, Ha T (2008) Spontaneous intersubunit rotation in single ribosomes. *Mol Cell* 30(5):578–588.
28. Ratje AH, et al. (2010) Head swivel on the ribosome facilitates translocation by means of intra-subunit tRNA hybrid sites. *Nature* 468(7324):713–716.
29. Guo ZJ, Noller HF (2012) Rotation of the head of the 30S ribosomal subunit during mRNA translocation. *Proc Natl Acad Sci USA* 109(50):20391–20394.
30. Savelsbergh A, et al. (2003) An elongation factor G-induced ribosome rearrangement precedes tRNA-mRNA translocation. *Mol Cell* 11(6):1517–1523.
31. Fei J, et al. (2009) Allosteric collaboration between elongation factor G and the ribosomal L1 stalk directs tRNA movements during translation. *Proc Natl Acad Sci USA* 106(37):15702–15707.
32. Tourigny DS, Fernández IS, Kelley AC, Ramakrishnan V (2013) Elongation factor G bound to the ribosome in an intermediate state of translocation. *Science* 340(6140): 1235490.
33. Chen H, Bjerknes M, Kumar R, Jay E (1994) Determination of the optimal aligned spacing between the Shine-Dalgarno sequence and the translation initiation codon of Escherichia coli mRNAs. *Nucleic Acids Res* 22(23):4953–4957.
34. Gavrilova LP, Kostiashkina OE, Koteliansky VE, Rutkevitch NM, Spirin AS (1976) Factor-free ("non-enzymic") and factor-dependent systems of translation of polyuridylic acid by Escherichia coli ribosomes. *J Mol Biol* 101(4):537–552.
35. Munro JB, Wasserman MR, Altman RB, Wang LY, Blanchard SC (2010) Correlated conformational events in EF-G and the ribosome regulate translocation. *Nat Struct Mol Biol* 17(12):1470–1477.
36. Chen J, Petrov A, Tsai A, O'Leary SE, Puglisi JD (2013) Coordinated conformational and compositional dynamics drive ribosome translocation. *Nat Struct Mol Biol* 20(6): 718–727.
37. Pan D, Kirillov SV, Cooperman BS (2007) Kinetically competent intermediates in the translocation step of protein synthesis. *Mol Cell* 25(4):519–529.
38. Munro JB, Sanbonmatsu KY, Spahn CM, Blanchard SC (2009) Navigating the ribosome's metastable energy landscape. *Trends Biochem Sci* 34(8):390–400.
39. Chen C, et al. (2013) Dynamics of translation by single ribosomes through mRNA secondary structures. *Nat Struct Mol Biol* 20(5):582–588.
40. Frank J, Gao H, Sengupta J, Gao N, Taylor DJ (2007) The process of mRNA-tRNA translocation. *Proc Natl Acad Sci USA* 104(50):19671–19678.
41. Qu X, et al. (2011) The ribosome uses two active mechanisms to unwind messenger RNA during translation. *Nature* 475(7354):118–121.
42. Namy O, Moran SJ, Stuart DI, Gilbert RJ, Brierley I (2006) A mechanical explanation of RNA pseudoknot function in programmed ribosomal frameshifting. *Nature* 441(7090):244–247.
43. Zhou J, Lancaster L, Donohue JP, Noller HF (2013) Crystal structures of EF-G-ribosome complexes trapped in intermediate states of translocation. *Science* 340(6140):1236086.
44. Pulk A, Cate JH (2013) Control of ribosomal subunit rotation by elongation factor G. *Science* 340(6140):1235970.